A Novel Strategy to Prevent Advanced Atherosclerosis and Lower Blood Glucose in a Mouse Model of Metabolic Syndrome

Jenny E. Kanter,[1] Farah Kramer,[1] Shelley Barnhart,[1] Jeffrey M. Duggan,[2,3] Masami Shimizu-Albergine,[1] Vishal Kothari,[1] Alan Chait,[1] Stephan D. Bouman,[4] Jessica A. Hamerman,[2,3] Bo F. Hansen,[5] Grith S. Olsen,[5] and Karin E. Bornfeldt[1,6]

Diabetes 2018;67:946–959 | https://doi.org/10.2337/db17-0744

Cardiovascular disease caused by atherosclerosis is the leading cause of mortality associated with type 2 diabetes and metabolic syndrome. Insulin therapy is often needed to improve glycemic control, but it does not clearly prevent atherosclerosis. Upon binding to the insulin receptor (IR), insulin activates distinct arms of downstream signaling. The IR-Akt arm is associated with blood glucose lowering and beneficial effects, whereas the IR-Erk arm might exert less desirable effects. We investigated whether selective activation of the IR-Akt arm, leaving the IR-Erk arm largely inactive, would result in protection from atherosclerosis in a mouse model of metabolic syndrome. The insulin mimetic peptide S597 lowered blood glucose and activated Akt in insulin target tissues, mimicking insulin's effects, but only weakly activated Erk and even prevented insulin-induced Erk activation. Strikingly, S597 retarded atherosclerotic lesion progression through a process associated with protection from leukocytosis, thereby reducing lesional accumulation of inflammatory Ly6C^{hi} monocytes. S597-mediated protection from leukocytosis was accompanied by reduced numbers of the earliest bone marrow hematopoietic stem cells and reduced IR-Erk activity in hematopoietic stem cells. This study provides a conceptually novel treatment strategy for advanced atherosclerosis associated with metabolic syndrome and type 2 diabetes.

Metabolic syndrome and type 2 diabetes (T2DM) are associated with increased cardiovascular disease (CVD) risk. Approximately one-third of the American population is estimated to have metabolic syndrome or prediabetes, which in turn increases the risk of developing T2DM. These states are frequently characterized by central obesity, elevated fasting blood glucose and insulin resistance, elevated blood pressure, and dyslipidemia, all of which have been postulated to play direct or indirect roles in exacerbating CVD. In addition to traditional risk factors, leukocytosis/monocytosis is associated with CVD (1,2). We have recently demonstrated that obesity and insulin resistance cause myelopoiesis (3).

T2DM and metabolic syndrome are characterized by impaired insulin sensitivity in insulin target tissues and, in the case of T2DM, an inability of islet β-cells to compensate for the decreased insulin sensitivity (4). Insulin therapy is often needed to improve glycemic control. Insulin receptor (IR) signaling has profound effects not only on insulin target tissues, such as liver, adipose tissue, and skeletal muscle, regulating blood glucose and plasma lipids, but also affects cells directly involved in atherosclerosis. Studies in mouse models demonstrate that loss of IRs can alter atherosclerosis through multiple mechanisms and multiple cell types. Thus, loss of hepatic IRs results in increased atherosclerosis through dyslipidemia (5), whereas low levels of hepatic IRs and loss of IR expression in all other tissues has the opposite effect (6). Lack of IRs in endothelial cells (7) exacerbates atherosclerosis, whereas lack of IRs in myeloid cells has different effects depending on the model (8,9).

[1]Division of Metabolism, Endocrinology and Nutrition, Department of Medicine, UW Medicine Diabetes Institute, University of Washington, Seattle, WA
[2]Department of Immunology, University of Washington, Seattle, WA
[3]Benaroya Research Institute, Seattle, WA
[4]Insulin Pharmacology, Novo Nordisk A/S, Måløv, Denmark
[5]Insulin Biology Department, Novo Nordisk A/S, Måløv, Denmark
[6]Department of Pathology, UW Medicine Diabetes Institute, University of Washington, Seattle, WA

Corresponding author: Karin E. Bornfeldt, bornf@uw.edu.

Received 25 June 2017 and accepted 1 February 2018.

This article contains Supplementary Data online at http://diabetes.diabetesjournals.org/lookup/suppl/doi:10.2337/db17-0744/-/DC1.

The discrepancies in pro- and antiatherogenic actions of IRs in different tissues might be explained by the fact that the IR induces distinct signaling pathways after activation. The IR activates two major pathways of signaling: the Akt axis and the Erk axis. Although a functional bifurcation of signaling events downstream of Akt has been shown to regulate hepatic lipogenesis versus gluconeogenesis (10), the relative roles of IR-induced Akt and Erk pathways on atherosclerosis are unknown.

To address this question, we took advantage of a selective IR agonist, with no structural homology with insulin, termed S597 (Ac-SLEEEWAQIECEVYGRGCPSESFYDWFERQL-amide). The IR is present on cells as a dimer. Each receptor monomer consists of a ligand-binding subunit (the α-subunit), a transmembrane domain, and an intracellular β-subunit with tyrosine kinase activity (11). Experimental data have been used to generate sophisticated models to explain the mechanism of insulin interaction with its receptor. These models describe two distinct sites on each IR α-subunit (12,13). Insulin activates the IR by binding to one site on one α-subunit and to the other site on another α-subunit. Peptide screening strategies have revealed that heterodimers consisting of peptide sequences that specifically bind to one or the other site have different biological properties, depending on the order of peptide linkage (13). One of these insulin mimetic peptides identified (13) is S597. S597's mechanism of IR binding effectively couples the IR to Akt signaling but is less effective in activating the IR-Erk axis in cell lines stably transfected with the human IR (14,15).

Using this peptide, we demonstrate that selective activation of the IR-Akt axis, leaving the IR-Erk pathway largely inactive, lowers blood glucose and protects against advanced atherosclerosis in an LDL receptor–deficient ($Ldlr^{-/-}$) mouse model of metabolic syndrome.

RESEARCH DESIGN AND METHODS

Animals and Treatments

These studies were approved by the University of Washington Institutional Animal Care and Use Committee and by Novo Nordisk A/S. Age-matched male $Ldlr^{-/-}$ mice (10–12 weeks of age on the C57BL/6J background) were obtained from The Jackson Laboratory (Bar Harbor, ME). Male mice were used because they develop a stronger metabolic syndrome phenotype than do female mice. The mice were fed chow (n = 5) or a diabetogenic diet with 0.15% cholesterol (DDC, No. F4997; Bio-Serv, Frenchtown, NJ) (16) for 4 weeks to initiate glucose intolerance and body weight gain. After a dose-finding study in separate mice and after the 4 weeks of DDC feeding, mice were randomized into three groups receiving twice-daily injections of vehicle, insulin (40 nmol/kg), or S597 (80 nmol/kg) (n = 15/group) for 4 or 18 weeks. They were randomized into three groups based on similar body weights (average 32 g), glucose levels (average 173 mg/dL), and cholesterol levels (average 707 mg/dL) in the three groups before initiation of vehicle, insulin, and S597 injections. Vehicle, human insulin, and S597 were produced specifically for this study at Novo Nordisk A/S, Måløv, Denmark, at a concentration resulting in 30–60 μL subcutaneous injections for insulin and S597, using NovoPens and needles. Glucose- and insulin-tolerance tests were performed as described (17).

Mice injected for 4 weeks were euthanized 7.5 or 15 min after their last injection to evaluate phosphorylation of Akt (p-Akt) and Erk (p-Erk) in liver, skeletal muscle (quadriceps), epididymal adipose tissue, aorta, and blood leukocytes using Alpha *Sure*Fire ELISAs (PerkinElmer, Waltham, MA). Additional mice from the S597-treated group were injected first with S597 and 7.5 min later were injected with insulin and euthanized 7.5 min later. For the 18-week study, S597 and insulin doses were adjusted weekly, based on body weight, and the blood glucose–lowering effects of insulin and S597 were evaluated every 4 weeks. Exclusion criteria were established before the beginning of the study: DDC-fed mice that had gained less weight than the average weight gain of chow-fed mice (115%) during the 18-week study were excluded. These criteria were used to exclude five mice from the study (two in the insulin group, two in the S597 group, and one in the vehicle group). In a third cohort of mice, $Ly6C^{hi}$ monocytes were labeled and traced into established atherosclerotic lesions after 10 days of vehicle, insulin, or S597 injections.

Flow Cytometry

Antibodies used for flow cytometry are described in the Supplementary Data Reagents Tables. Directly after a CD16/CD32 block, a combination of antibodies (FITC-CD45, PE-CD115, PE-Cy7-GR1, APC-B220, APC-CD3e, and PerCy5.5-CD11B) was added to blood leukocytes and incubated for 30 min on ice. The cells were then washed twice and fixed in 1% neutral buffered paraformaldehyde for 15 min. The cells were analyzed on a BD FACSCanto RUO (BD Biosciences, San Jose, CA). Monocytes were identified as $CD45^+$ $B220^-$ $CD3e^-$ $CD115^+$ cells. $GR1^{hi}$ and $GR1^{lo}$ cells identified the two monocyte populations $Ly6C^{hi}$ and $Ly6C^{lo}$ (Supplementary Fig. 1*A* and *B*). Neutrophils were identified as $CD115^-$ $GR1^+$ $B220^-$ $CD3e^-$ cells. Bone marrow progenitor cell populations were analyzed as previously described (18). Emergency granulocyte-macrophage progenitors (eGMP) were identified as $Lineage^-$ $CD117^+$ $Sca\text{-}1^+$ $CD16/32^{hi}$ $CD34^+$ cells (Supplementary Fig. 1*C*). In some experiments, LSK ($Lineage^-$ $CD117^+$ $Sca\text{-}1^+$) cells were sorted on a BD FACSAria and then stimulated for 7.5 min with vehicle, insulin, or S597. The cells were stained for intracellular p-Erk (Thr202/Tyr204) and analyzed on a BD LSR II.

Monocyte Tracing Studies

$Ldlr^{-/-}$ mice were fed DDC for 16 weeks to establish atherosclerotic lesions. The mice were then injected with vehicle, insulin, or S597 for 10 days. On day 10, monocytes were depleted by retro-orbitally injecting clodronate liposomes (Standard Macrophage Depletion Kit; Encapsula NanoSciences; 200 μL/mouse at 5 mg/mL of clodronate; Thermo Fisher Scientific, Pittsburg, PA). Blood monocytes were depleted by 89.7 ± 0.7%, $Ly6C^{hi}$ monocytes by 85.1 ± 1.2%, and $Ly6C^{lo}$ monocytes by 95.3 ± 0.3% 18 h after

clodronate injection compared with nonclodronate-injected control. After verification (18 h after clodronate injection) of monocyte depletion, yellow-green (YG) microsphere beads (Fluoresbrite YG Microspheres 0.5 μm; Fisher Scientific) were injected to selectively label Ly6C^{hi} monocytes (19). Recruitment of bead-positive cells was analyzed 3 days after bead injection. Briefly, aortas were dissected, fixed, embedded in optimal cutting temperature compound, and sectioned longitudinally. Presence of lesions was determined across the aorta using a Movat pentachrome stain, and sections adjacent to sites of identified lesions were stained with an anti-CD68 antibody (Bio-Rad Antibodies, Raleigh, NC), mounted with DAPI-containing media, and visualized. YG particles in CD68$^+$ lesion areas were counted by an investigator blinded to the treatment groups.

Human Hematopoietic Stem Cells

CD34$^+$ progenitor cells from four separate donors (PromoCell, Heidelberg, Germany) were expanded for 10–14 days and then stimulated with vehicle, insulin (100 nmol/L), or S597 (200 nmol/L) for 7.5 min. Cells were immediately fixed, permeabilized, stained for intracellular p-Erk and cell surface CD34 and CD38, and analyzed on a Canto RUO. The mean from each donor (n = 2–5 replicates/donor) was analyzed.

Western Blots, ELISAs, and S597 Binding Studies

Antibodies used for Western blots are described in the Supplementary Data. The total Erk1/2 antibody was a rabbit polyclonal (20). p-Akt1/2/3 ELISAs were from Cell Signaling. The endothelin 1 ELISA was from Enzo Life Sciences (Farmingdale, NY). Plasma serum amyloid A levels were measured as described previously (21). Screening of S597's ability to displace ligands from receptors and binding sites was performed by Ricerca Biosciences, LLC (Taipei, Taiwan). For analysis of IR and IGF-I receptor levels by Western blot, a standard curve was generated for each gel using cell lines expressing known numbers of IRs and IGF-I receptors (22). Hepa 1-6 cells (ATTC CRL-1830TM) were obtained from American Type Culture Collection (Manassas, VA).

Analysis of Atherosclerosis

The mice were euthanized after 24 weeks and gently perfused with PBS, and the aorta and brachiocephalic artery (BCA) were dissected. After removal of the BCA, the aorta was flushed with RNAlater (Life Technologies, Grand Island, NY) and then placed in RNAlater. The aortas were opened longitudinally, and atherosclerosis was determined en face in a masked fashion. Aortic lipids and RNA were extracted as described by Akopian and Medh (23). Aortic cholesterol and triglycerides were measured using fluorescent and colorimetric assays, respectively (Cayman Chemical, Ann Arbor, MI, and Sigma-Aldrich, St. Louis, MO). The entire length of the BCA was serially sectioned, and every 30 μm, two cross sections were stained using a Movat pentachrome stain (24) for quantification of maximum lesion area and lesion morphological analysis. BCA cross sections adjacent to the maximal lesion site were stained with antibodies and reagents described in the Supplementary Data Reagents Tables or in previous studies (24–26). Real-time quantitative PCR was performed as described (26). Primer sequences are listed in the Supplementary Data Primer Table.

Plasma and Blood Analyses

Plasma mouse insulin levels were measured using an ultrasensitive rat insulin ELISA (cat. no. 90600; Crystal Chem, Downers Grove, IL), which has 100% cross-reactivity with mouse insulin. Interleukin (IL) 6, MCP-1, and tumor necrosis factor-α (TNF-α) plasma levels were measured using the Milliplex multiplex assay (EMD Millipore, Billerica, MA). Blood and plasma cholesterol, plasma triglycerides, glucose, and lipoprotein profiles were analyzed as previously described (21,24). Plasma cholesterol and glycohemoglobin were measured using colorimetric kits from Wako (Richmond, VA) and Fisher Scientific, respectively. Human LDL was isolated and acetylated according to previously described methods (27).

In Vitro Stimulation of Cells

Unless otherwise stated, in vitro stimulation of cells used 100 nmol/L insulin and 200 nmol/L S597. The higher concentration of S597 was used to mimic the in vivo studies, based on equi-effective blood glucose–lowering effects of insulin and S597. Mouse aortic and heart endothelial cells were harvested as previously described (28,29). For monocyte-endothelial adhesion assays, the endothelial cells were stimulated in the presence or absence of 20 ng/mL mouse recombinant TNF-α (R&D Systems, Minneapolis, MN) and vehicle, insulin, or S597 for 4 h, followed by extensive washing and addition of primary mouse bone marrow monocytes (monocyte enrichment kit; Stemcell Technologies, Vancouver, Canada) that had been labeled with calcein-acetoxymethyl ester (Sigma-Aldrich) for 30 min at 37°C. Monocyte adhesion was estimated based on emitted fluorescence. Thioglycollate-elicited macrophages and bone marrow cells were harvested as previously described (26). Bone marrow–derived macrophages were differentiated in the presence of 30% L-cell conditioned medium for 7 days, followed by M1 (5 ng/mL lipopolysaccharide [LPS] + 12 ng/mL interferon-γ [IFN-γ]) or M2 (4 ng/mL IL-4) stimulation (24 h), as previously described (17), in the presence of vehicle, 100 nmol/L insulin, or 200 nmol/L S597. Thioglycollate-elicited macrophages were harvested and stimulated with vehicle or 100 μg/mL acetylated LDL (AcLDL) or AcLDL together with 10 μg/mL of the acyl coenzyme A (CoA):cholesterol acyltransferase (ACAT) inhibitor 58035 for 24 h. Assays of cell death, as measured by TUNEL staining (TiterTACS; R&D Systems), were performed 24 h after stimulation. 3T3-L1 murine preadipocytes were differentiated into mature adipocytes (30) and then incubated in serum-free medium for 48 h, followed by stimulation with vehicle, insulin, and/or S597.

Statistical Analysis

Power calculations were used to determine the number of animals per group. Investigators were blinded to the group

allocation. Statistical analysis was performed using two-tailed unpaired Student *t* tests or one-way ANOVA with Tukey multiple comparison post hoc tests or two-way ANOVA for normally distributed data. For nonparametric parameters, Kruskal-Wallis or Dunn multiple comparison tests were used, as appropriate. Groups analyzed by *t* test had similar variance. Probabilities of <0.05 were considered statistically significant. In vitro experiments were performed at least three times in independent experiments.

RESULTS

S597, but Not Insulin, Slows Progression of Atherosclerosis

To investigate whether S597 affects the development of atherosclerosis, $Ldlr^{-/-}$ mice fed chow or DDC were treated with twice-daily injections of vehicle, insulin (40 nmol/kg), or S597 (80 nmol/kg) for 18 weeks (Fig. 1*A*). The extent of atherosclerosis was evaluated in the aorta and the BCA, a site known to develop advanced lesions (31). DDC-fed mice had more aortic atherosclerosis than chow-fed mice, as determined by en face analysis (representative aortas are shown in Fig. 1*B*). Insulin treatment did not alter the aortic atherosclerotic area; however, S597-treated mice had a significant reduction in the extent of atherosclerosis and aortic cholesterol and cholesteryl ester accumulation, without differences in aortic triglycerides (Fig. 1*B–G*). Mice fed DDC also exhibited large advanced BCA lesions (Fig. 1*H–J*). As in the aorta, S597 reduced BCA lesion size compared with vehicle and insulin (Fig. 1*H* and *I*).

To gain further insight into the mechanism whereby S597 protects against atherosclerosis, we evaluated BCA lesion morphology (Fig. 1*J*). Lesions were characterized by the presence and thickness of fibrous caps, intraplaque hemorrhage, collagen, glycosaminoglycans, necrotic cores, cholesterol clefts, calcification, and chondrocyte-like cells. Lesions from mice receiving S597 had fewer necrotic cores, suggesting that S597 protects against the formation of advanced lesions (Fig. 1*J* and *K*). Reductions in TUNEL and cleaved caspase-3, markers of cell death, were also observed in lesions from animals treated with S597 (Fig. 1*L* and *M*). Furthermore, S597 treatment resulted in a concomitant increase in intact macrophages in the core area of the lesions without altering the relative content of lesional macrophages (Fig. 1*N* and *O*). There were no differences in lesional smooth muscle accumulation, markers of proliferation, or expression of inflammatory mediators (Fig. 1*P* and Supplementary Fig. 2*A–E*).

Because necrotic cores are caused largely by macrophage death, these results suggest that S597 protects lesional macrophages from death and/or that lesional macrophage accumulation is slower. The latter explanation was supported by the selectively reduced levels of *Emr1* mRNA (F4/80; a macrophage marker) in aortas of S597-treated mice (Supplementary Fig. 2*E–G*). In addition, a series of experiments in isolated macrophages confirmed that S597 does not directly protect against macrophage cell death, lipid accumulation, or inflammatory properties of these cells. Thus, neither insulin nor S597 resulted in altered expression of cytokines or markers of activation in thioglycollate-elicited peritoneal macrophages under basal conditions or in bone marrow–derived macrophages induced by LPS+IFN-γ or IL-4 to take on M1 or M2 phenotypes, respectively (Fig. 2*A–G*). Furthermore, neither insulin nor S597 altered free cholesterol or cholesteryl ester levels in macrophages under basal conditions or in macrophage foam cells induced by incubation with AcLDL or AcLDL plus an ACAT inhibitor, which results in elevated levels of free cholesterol (Fig. 2*H* and *I*) or in increased apoptosis induced by three different stimuli (Fig. 2*J*). Together, these results suggest that the slowed macrophage accumulation in S597-treated mice is not a direct effect of S597 on lesional macrophages.

Mouse studies have revealed that the IR prevents monocyte recruitment via reduced expression of the monocyte adhesion molecule vascular cell adhesion molecule 1 (VCAM-1) in endothelial cells (7). *Vcam1* was upregulated in aortas of DDC-fed mice, but neither insulin nor S597 resulted in a significant reduction of aortic *Vcam1*, of *Vcam1* in isolated aortic endothelial cells, or in monocyte adhesion to endothelial cells (Fig. 2*K–M*). Insulin and S597 also did not acutely alter secretion of endothelin 1, a potent vasoconstrictor, from endothelial cells (Fig. 2*N*) or aortic endothelin 1 (*Edn1*) mRNA levels (data not shown). Furthermore, S597, over a broad range of concentrations, failed to activate Akt1, Akt2, and Akt3 in isolated endothelial cells or macrophages measured by ELISA or Western blot analysis (Fig. 2*O* and *P* and Supplementary Fig. 3, and data not shown). Neither insulin nor S597 resulted in significant activation of Erk in endothelial cells, consistent with previous studies on insulin effects in these cells (7). The failure of S597 to directly activate vascular cells might be explained by low numbers of IRs compared with, for example, hepatocytes, adipocytes, and skeletal muscle. Another possibility is that the presence of IR–IGF-I receptor hybrids (32,33) hinders the effects of S597 because S597 fails to activate the IGF-I receptor (14). Indeed, aortic endothelial cells expressed approximately half the number of IRs but many more IGF-I receptors than did hepatocytes. Thioglycollate-elicited macrophages expressed even fewer IRs (Fig. 2*Q*). Together, our results suggest that S597 prevents the formation of advanced lesions of atherosclerosis through a mechanism that involves reduced accumulation of lesional macrophages and is unlikely to be due to activation of IRs on vascular cells.

S597 Lowers Blood Glucose but Does Not Alter Plasma Cholesterol or Systemic Inflammation

Mice fed DDC were obese and glucose intolerant 4 weeks after diet initiation (Fig. 3*A*). S597 acutely lowered blood glucose to the same extent and with the same time course as did insulin at the beginning and at the end of the study (Fig. 3*B* and *C*), demonstrating that the mice did not become desensitized to S597. Neither insulin nor S597 affected body weights, glycohemoglobin, fasting blood glucose, nonfasting blood glucose, or plasma insulin levels (Fig. 3*D–G* and Supplementary Fig. 4*A* and *B*), likely because

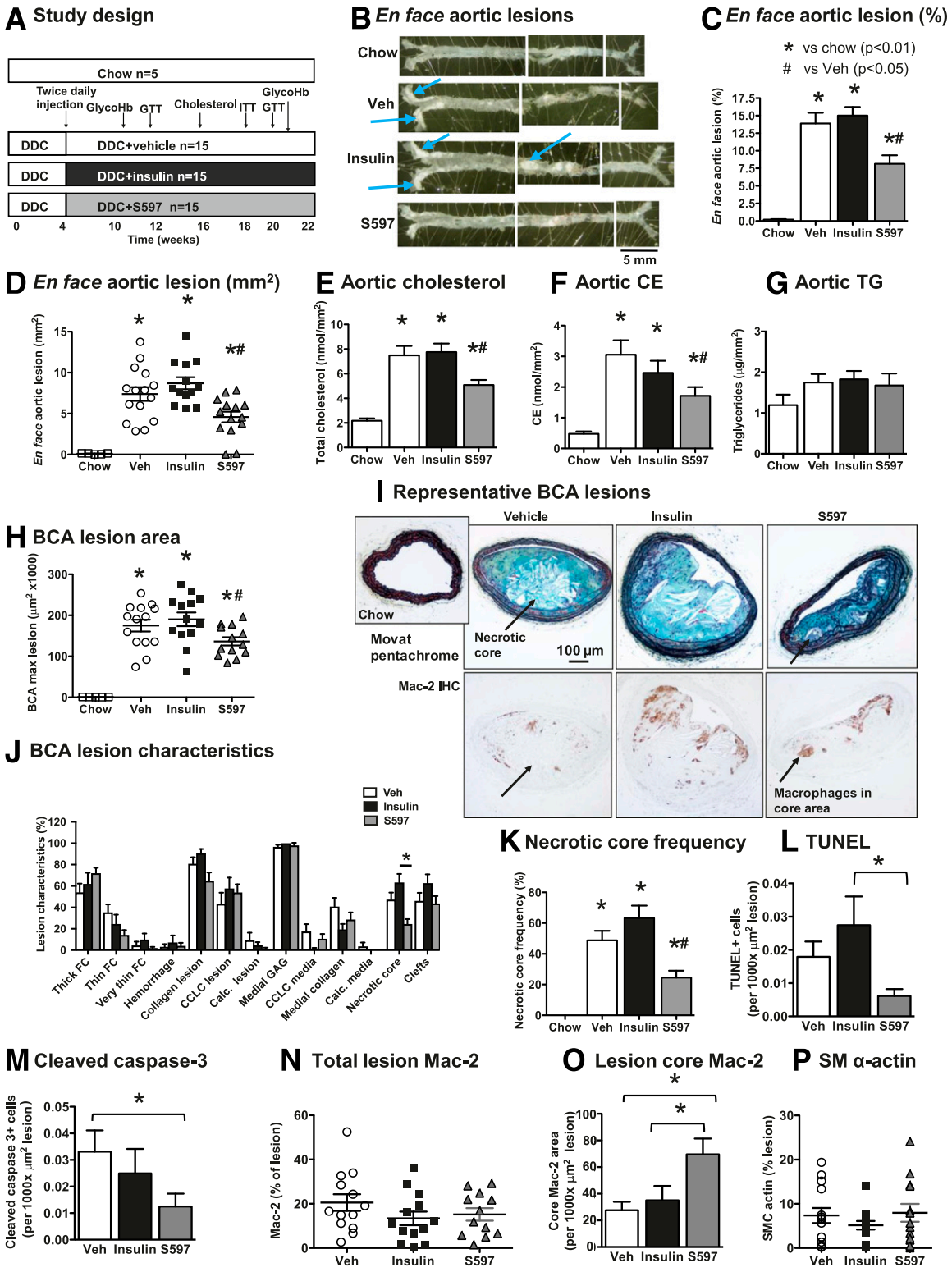

Figure 1—S597 prevents advanced atherosclerosis in a mouse model of metabolic syndrome. Male *Ldlr*$^{-/-}$ mice were fed chow or a DDC for 4 weeks and then were treated with vehicle (Veh), insulin (40 nmol/kg), or S597 (80 nmol/kg) twice daily for an additional 18 weeks. First, a dose-finding study in which the dose of S597 resulting in a similar blood glucose–lowering effect as that of 40 nmol/kg regular human insulin was performed by monitoring blood glucose lowering for up to 240 min in mice injected subcutaneously with different doses of S597. The dose of S597 was gradually increased in different sets of mice until the equi-effective dose of 80 nmol/kg was identified. *A*: Schematic of study design. At the end of the study, the aorta and the BCA were dissected. GlycoHb, glycohemoglobin; GTT, glucose tolerance test; ITT, insulin tolerance test. *B*: Representative examples of en face preparations of aortas. Examples of atherosclerotic lesions are indicated by blue arrows. The extent of atherosclerosis was determined en face in the aortas and expressed as percentage of total aortic area (*C*) or as square millimeters (*D*). Lipids were extracted from the same aortas, and total cholesterol (*E*), cholesteryl esters (CE) (*F*), and triglycerides (TG) (*G*) were measured. *H*: The

of the transient blood glucose–lowering effects (2–3 h) of twice-daily subcutaneous S597 and insulin injections (Fig. 3*B* and *C*). Neither insulin nor S597 resulted in an overall improvement of glucose tolerance in DDC-fed mice (Fig. 3*H–K*) or altered plasma insulin levels at 30 min after glucose injection (Fig. 3*L*). Likewise, overall insulin tolerance was not altered by S597 or insulin in DDC-fed mice (Fig. 3*M* and *N*). DDC-fed mice were moderately insulin resistant, measured as a reduced ability of insulin to activate hepatic Akt and GSK3β in DDC-fed mice compared with chow-fed mice, and this again was not altered by insulin or S597 (Fig. 3*O* and *P*). Consistently, expression of hepatic genes involved in gluconeogenesis and lipid metabolism were not significantly altered (Supplementary Fig. 4*C–F*).

Neither insulin nor S597 significantly altered plasma lipids at the end of the 18-week study (Fig. 4*A–D*). In agreement with recent findings in Zucker diabetic fatty rats, which were continuously treated with S597 through osmotic mini-pumps for 7 days (34), a shorter 4-week treatment with S597 revealed reduced levels of plasma triglycerides, but not plasma cholesterol, in S597-treated mice (Fig. 4*F* and *G*). Importantly, aortic lesion area did not correlate with plasma triglycerides (Supplementary Fig. 4*G*), suggesting that triglyceride lowering does not explain the reduced atherosclerosis in S597-treated mice, consistent with the inconclusive results of triglyceride-lowering on CVD in humans (35). Moreover, neither insulin nor S597 altered plasma inflammatory mediators (Fig. 4*E*). Therefore, insulin and S597 have acute blood glucose–lowering effects but have no major effects on obesity, insulin resistance, systemic inflammatory mediators, or cholesterol profiles in this model of metabolic syndrome, suggesting that the reduced atherosclerosis observed with S597 is not due to effects on these parameters.

S597 Preferentially Activates Akt Over Erk and Prevents Insulin-Induced Erk Activation

We next confirmed that S597 stimulation leads to Akt phosphorylation rather than Erk phosphorylation in 3T3-L1 cells differentiated into mature adipocytes, as has previously been shown in cell lines overexpressing the IR (14,15). Indeed, S597 (200 nmol/L) resulted in Akt phosphorylation equaling that of insulin (100 nmol/L) but resulted in an ~50% lower Erk phosphorylation compared with insulin over a wide range of concentrations and time points investigated (Supplementary Fig. 5*A–D*). Furthermore, S597 inhibited the ability of insulin to activate Erk but did not impair insulin's ability to activate Akt (Supplementary Fig. 5*A* and *B*). These results are consistent with a model in which S597 results in preferential activation of the IR-Akt arm of signaling and reduced IR-Erk activation, potentially due to a slower IR internalization in S597-stimulated cells (14,15). Because S597 binds the IR with higher affinity than does insulin (15), under conditions in which insulin and S597 are both present, Akt activation remains intact whereas Erk activation is impaired (Fig. 5*A*).

We next asked whether S597 would preferentially activate Akt over Erk in our mouse model of metabolic syndrome. *Ldlr*$^{-/-}$ mice were fed chow or DDC for 4 weeks, and DDC-fed mice were then injected twice daily with vehicle, insulin (40 nmol/kg), or S597 (80 nmol/kg) for an additional 4 weeks. Levels of p-Akt and p-Erk were analyzed in different tissues 7.5 and 15 min after the last injection. To test the ability of S597 to prevent insulin-induced Erk activation, one group of mice received S597 and 7.5 min later received insulin for 7.5 min. Consistent with the 3T3-L1 adipocyte cell data, insulin induced a significant increase in p-Erk in adipose tissue, whereas the effect of S597 was lower (Fig. 5*B*). Furthermore, the ability of insulin to induce p-Erk was prevented by S597 (Fig. 5*B*). Levels of p-Erk were low in skeletal muscle in all groups (Fig. 5*C*), and neither insulin nor S597 induced significant hepatic p-Erk, p-p38 MAPK, or p-JNK (Fig. 5*D* and Supplementary Fig. 6*A–C*).

Conversely, insulin and S597 caused a similar extent of Akt phosphorylation in adipose tissue and skeletal muscle, and S597 also stimulated p-Akt in liver although not to the same extent. Importantly, S597 did not prevent the ability of insulin to activate Akt (Fig. 5*E–G*). In the aorta, neither insulin nor S597 stimulated p-Erk (Fig. 5*H*). Insulin significantly stimulated p-Akt whereas S597 did not (Fig. 5*I*), consistent with our finding in isolated endothelial cells and macrophages (Fig. 2*O* and *P*), and S597 even appeared to inhibit the effect of insulin on p-Akt in aortic tissue. Insulin and S597 did not affect p-Erk or p-Akt in pooled blood leukocytes (Fig. 5*J* and *K*).

The IR was the only receptor detected to which S597 binds with high affinity of the 163 receptors and transporters that were screened (Supplementary Table 1). Thus, S597

maximal cross-sectional lesion area in the BCA was determined from each animal, and the average maximal lesion area is presented. *I*: Representative BCA cross sections stained using Movat pentachrome stain (upper panels) or an anti–Mac-2 antibody for macrophage quantification (lower panels). IHC, immunohistochemistry. *J*: BCA cross sections were scored for frequency of lesion characteristics. Different lesion characteristics were evaluated throughout the entire length of the BCA using the Movat pentachrome-stained sections. Presence or absence of each characteristic was scored on each section, and the percentage of positive sections for each animal over the length of the artery (20–25 sections per mouse) is reported: thick fibrous cap (FC) >10 layers, thin FC 5–10 layers, and very thin FC <5 layers above the necrotic core. Hemorrhage scored positive as bright red stain and the presence of erythrocytes. Calc., calcification; CCLC, chondrocyte-like cells; Clefts, cholesterol clefts; GAG, glycosaminoglycans. *K*: Necrotic core frequency. BCA sections adjacent to the maximal lesion site were stained for TUNEL (*L*), cleaved caspase-3 (*M*), or total macrophages, using a Mac-2 antibody (*N*). *O*: The Mac-2–positive macrophage area was also quantified in the lesion core. *P*: Quantification of smooth muscle (SM) α-actin stain in BCA lesions. SMC, smooth muscle cell. Data are expressed as mean ± SEM (chow: $n = 5$; DDC groups: vehicle, $n = 14$; insulin, $n = 13$; S597, $n = 13$). *$P < 0.05$ vs. chow; #$P < 0.05$ vs. vehicle, as indicated by one-way ANOVA.

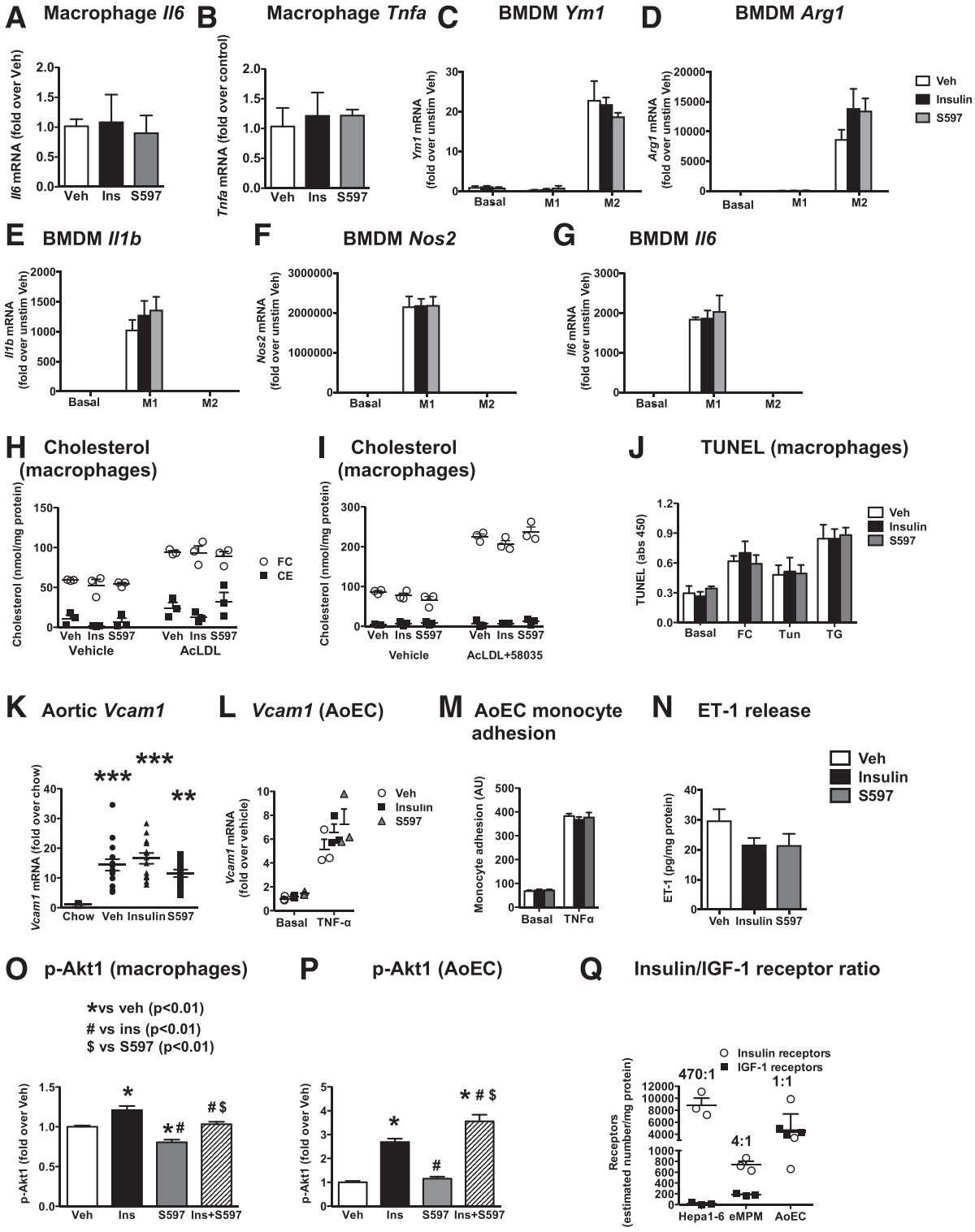

Figure 2—S597 has no detected direct effects on isolated macrophages and endothelial cells. All in vitro studies were performed with vehicle (Veh), insulin (Ins; 100 nmol/L), or S597 (200 nmol/L). *A* and *B*: Thioglycollate-elicited macrophages (n = 3) were harvested and adhesion purified for 1 h, followed by stimulation for 18 h. Cytokine mRNA levels, *Il6* (*A*) and *Tnfa* (*B*), were measured by real-time PCR. *C*–*G*: Bone marrow–derived macrophages (BMDM; n = 3) were differentiated for 7 days in the presence of L-cell conditioned medium, followed by M1 (5 ng/mL LPS + 12 ng/mL IFN-γ) or M2 (4 ng/mL IL-4) stimulation, or no additional stimulation (Basal) for 24 h in the presence of vehicle, insulin, or S597. *C*: *Ym1* mRNA, an M2 marker. *D*: *Arg1* mRNA, an M2 marker. *E*: *Il1b* mRNA, an M1 marker. *F*: *Nos2* mRNA, an M1 marker. *G*: *Il6* mRNA, an M1 marker. *H* and *I*: Thioglycollate-elicited macrophages (n = 3) were harvested and stimulated with vehicle or 100 μg/mL AcLDL (*H*) or AcLDL together with 10 μg/mL ACAT inhibitor 58035 for 24 h (*I*) in the presence or absence of insulin or S597. Free cholesterol (FC) and cholesteryl esters (CE) were extracted and measured. Macrophages were stimulated with 100 μg/mL AcLDL or loaded with free cholesterol, using 100 μg/mL AcLDL during ACAT inhibition (compound 58035, 10 μg/mL; Sigma-Aldrich). *J*: Assays of cell death, as measured by TUNEL staining (TiterTACS; R&D Systems), were performed 24 h after stimulation. abs 450, absorbance 450 nm; FC, free cholesterol loading; Tun, tunicamycin (5 μg/mL); TG,

preferentially activates the IR-Akt signaling arm over Erk signaling in insulin target tissues and, in addition, prevents insulin-induced Erk activation.

S597 Prevents Leukocytosis and Increased Levels of Ly6C^{hi} Monocytes Associated With the Metabolic Syndrome Phenotype

There is a link between increased leukocytosis/monocytosis and CVD in humans and mice (1,36,37), and insulin resistance and obesity promote leukocytosis through increased adipose tissue inflammation (3,38–40). Consistently, DDC feeding induced marked leukocytosis (Fig. 6*A–E* and Supplementary Fig. 7*A–C*). The main stimulatory effect of DDC feeding was observed for Ly6C^{hi} monocytes. S597 treatment prevented DDC-induced leukocytosis, whereas insulin had no effect. Interestingly, the reduction induced by S597 was most clearly observed in the inflammatory Ly6C^{hi} monocyte population, in which S597 normalized the levels to those seen in chow-fed mice (Fig. 6*C*).

S597 Reduces Ly6C^{hi} Monocyte Accumulation in Atherosclerotic Lesions and Suppresses Bone Marrow Hematopoietic Stem Cells and Erk Activation in These Cells

To test whether fewer circulating Ly6C^{hi} monocytes results in fewer monocytes accumulating in lesions, we selectively labeled newly formed Ly6C^{hi} monocytes using microsphere beads and traced them into aortic lesions (Fig. 6*F* and *G*). Four days after monocyte depletion, blood Ly6C^{hi} monocyte levels had returned to normal but remained lower in S597-treated mice. Accordingly, the lesions of S597-treated mice exhibited fewer recruited bead-labeled macrophages (Fig. 6*H*).

Because leukocytosis/monocytosis associated with atherosclerosis has been associated with bone marrow hematopoiesis (2,37,41), we next investigated whether S597 reduced hematopoiesis. The number of bone marrow long-term hematopoietic stem cells was lower in S597-treated mice than in insulin-treated mice (Fig. 6*I*). In addition, S597-treated mice exhibited reduced numbers of an inflammation-induced granulocyte-macrophage progenitor with high differentiation capacity, the eGMP (18), compared with insulin-treated mice (Supplementary Fig. 7*D*). Concomitantly, S597 reduced p-Erk in mouse hematopoietic stem cells (Fig. 6*J* and Supplementary Fig. 7*E*) and also exhibited a modest suppressive effect in human CD34^{+} hematopoietic stem cells (Supplementary Fig. 7*F*), suggesting that the effect of S597 might be of human relevance.

DISCUSSION

This study reveals that the insulin mimetic peptide S597 causes differential activation of IR-Akt over IR-Erk and, as a result, hinders insulin-induced Erk activation, lowers blood glucose, and protects against formation of advanced atherosclerosis in a mouse model of metabolic syndrome. The only previous study on the effects of S597 in vivo used osmotic mini-pumps to continuously administer S597 to Zucker diabetic fatty rats during a 7-day period to evaluate its effects on blood glucose, hepatic lipid metabolism, adiposity, and plasma lipids (34). That study found S597 lowered blood glucose and plasma triglyceride levels, caused weight gain, and reduced hepatic de novo synthesis of fatty acids (34). Consistent with that study, we found a transient effect of S597 treatment on plasma triglycerides and no effect on plasma cholesterol. The lack of effects of S597 on body weight in the current study is most likely a result of the transient effects of the twice-daily subcutaneous injections and possibly the longer study duration. Use of osmotic mini-pumps was not feasible in the present 18-week atherosclerosis study. This is the first study to evaluate the effects of S597 on the vasculature.

Some of the beneficial effects of S597 are likely to be due to Akt activation in insulin target tissues, such as its ability to mimic insulin's blood glucose–lowering effects. Other beneficial effects of S597 are likely a result of its ability to prevent IR-Erk activation by insulin. The concept that IR-Akt activation results in antiatherogenic effects, whereas IR-Erk activation is proatherogenic, is in line with findings of King et al. (42). Thus, we demonstrate that S597 prevents advanced atherosclerosis in the mouse model of metabolic syndrome, concomitant with a marked protection from Ly6C^{hi} monocytosis in this model. On one hand, Ly6C^{hi} monocytes are monocytes recruited from the bone marrow in response to inflammatory stimuli, and this population readily enters lesions of atherosclerosis (19). Ly6C^{lo} monocytes, on the other hand, are patrolling monocytes involved in tissue repair (43).

The antiatherogenic effects of S597 are likely to be at least partly due to its ability to prevent diet-induced leukocytosis and Ly6C^{hi} monocytosis through inhibition of

thapsigargin (5 μmol/L). *K*: Aortic *Vcam1* mRNA. Data were normalized to *Rn18s* values and presented using the ΔΔCT method with the chow group as controls (chow: $n = 5$; DDC groups: vehicle, $n = 14$; insulin, $n = 13$; S597, $n = 13$). Similar results were obtained when the data were normalized to *Rpn32* or *Gapdh*. $^{**}P < 0.01$; $^{***}P < 0.001$. *L–N*: Primary mouse aortic endothelial cells (AoEC) or heart endothelial cells (*N*) were stimulated with 20 ng/mL TNF-α in the presence and absence of insulin or S597. *L*: Endothelial cell *Vcam1* mRNA. *M*: Primary mouse bone marrow monocytes were added to a monolayer of endothelial cells, and adhesion of monocytes to the endothelium was determined. AU, arbitrary units. *N*: Endothelin 1 (ET-1) release 20 min after insulin or S597 stimulation. *O*: Isolated thioglycollate-elicited macrophages (eMPM) were stimulated with vehicle (PBS), 100 nmol/L insulin, 200 nmol/L S597, or a combination of 100 nmol/L insulin and 200 nmol/L S597 for 15 min. Samples were analyzed using p-Akt1–specific ELISAs ($n = 6–9$). *P*: Aortic endothelial cells were stimulated with vehicle, 100 nmol/L insulin, 200 nmol/L S597, or a combination of 100 nmol/L insulin and 200 nmol/L S597 for 15 min and analyzed for p-Akt1. Data are expressed as mean ± SEM ($n = 5$). Symbol definitions in panel *O* also apply to *P*. *Q*: Hepa1-6 cells, AoECs, and eMPMs were harvested and analyzed for expression of the IR and IGF-1 receptor ($n = 3$). None of the cell lines used in this study is included in the database of commonly misidentified cell lines (International Cell Line Authentication Committee). Cells were free of mycoplasma contamination, as determined by the MycoProbe Mycoplasma Detection Kit (R&D Systems).

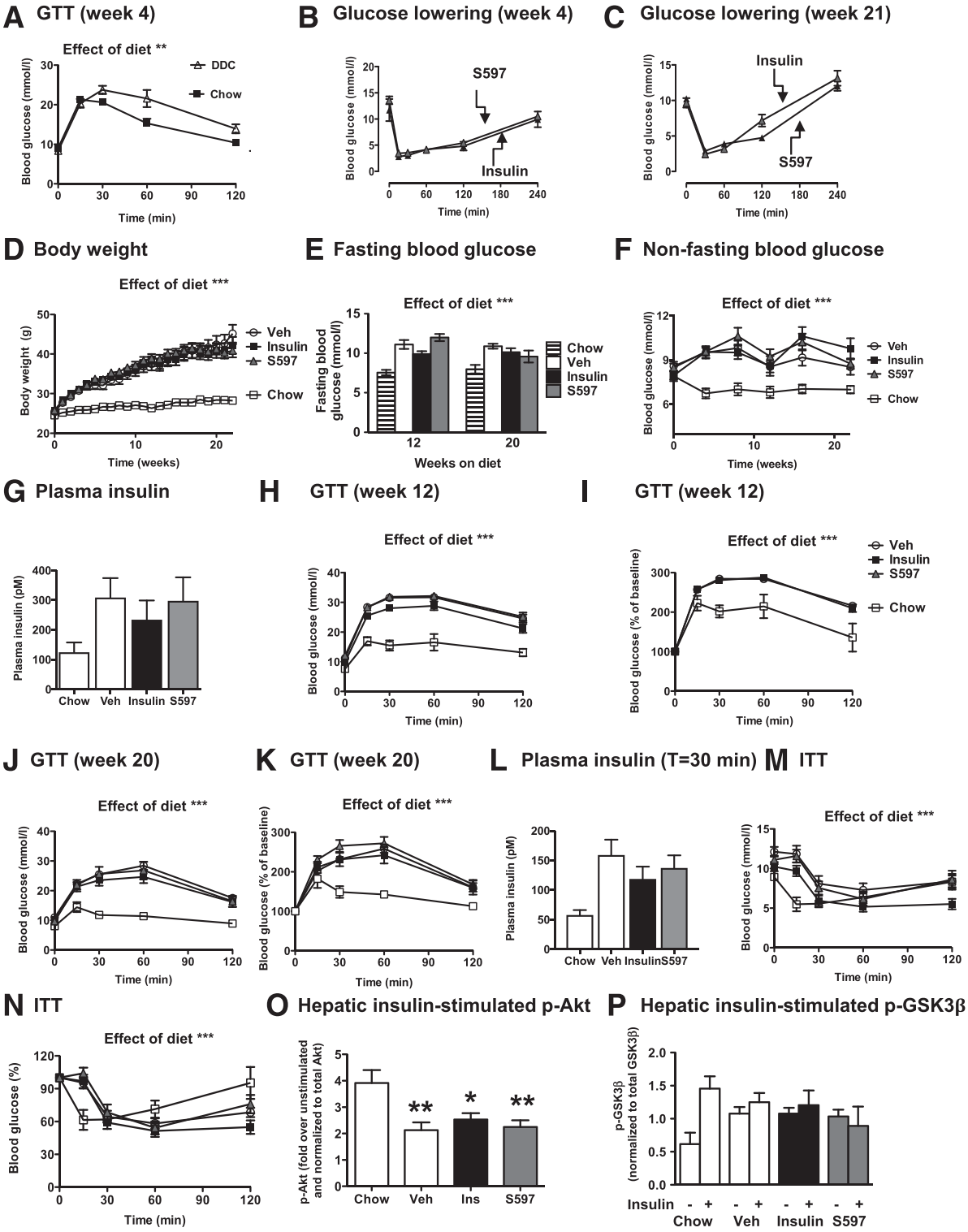

Figure 3—S597 acutely lowers blood glucose but does not affect the overall metabolic syndrome–like phenotypes. *A*: Mice were fed the DDC for 4 weeks and then underwent an intraperitoneal glucose tolerance test (GTT) (1.5 mg/g D-glucose at week 4) after a fast of 4–6 h. Blood glucose was monitored at the indicated times. *B* and *C*: Acute blood glucose–lowering effects of insulin and S597 were evaluated every 4 weeks to confirm that the effects were not waning over time. Blood glucose lowering at week 4 ($n = 3$) (*B*) and week 21 (*C*). *D*: Body weights measured weekly throughout the study. Veh, vehicle. *E*: Fasting blood glucose at 12 and 20 weeks. *F*: Nonfasting blood glucose throughout the study. Glucose was measured in the morning (7:00 A.M.), 14.5 h after the previous S597 and insulin injections (4:30 P.M. the previous day). *G*: Plasma insulin at the end of the study. *H–K*: Intraperitoneal GTTs at 12 weeks (*H* and *I*) and 20 weeks (*J* and *K*), similar to *A* but using 1.0 mg/g D-glucose at week 20. Absolute blood glucose values (*H* and *J*) and percentage of baseline values (*I* and *K*) are shown. *L*: Plasma insulin at 30 min during the 20-week GTT. Note that these are not the same ELISAs as in *G*. *M* and *N*: Insulin tolerance tests (ITTs) were performed in a manner similar to the GTTs at week 18, but 1.2 mU/g human regular insulin was injected intraperitoneally. *M*: Absolute blood glucose values. *N*: Glucose as percentage of baseline values. At the end of the study, a subset of animals was injected with insulin (1.2 mU/g) or vehicle 8 min before

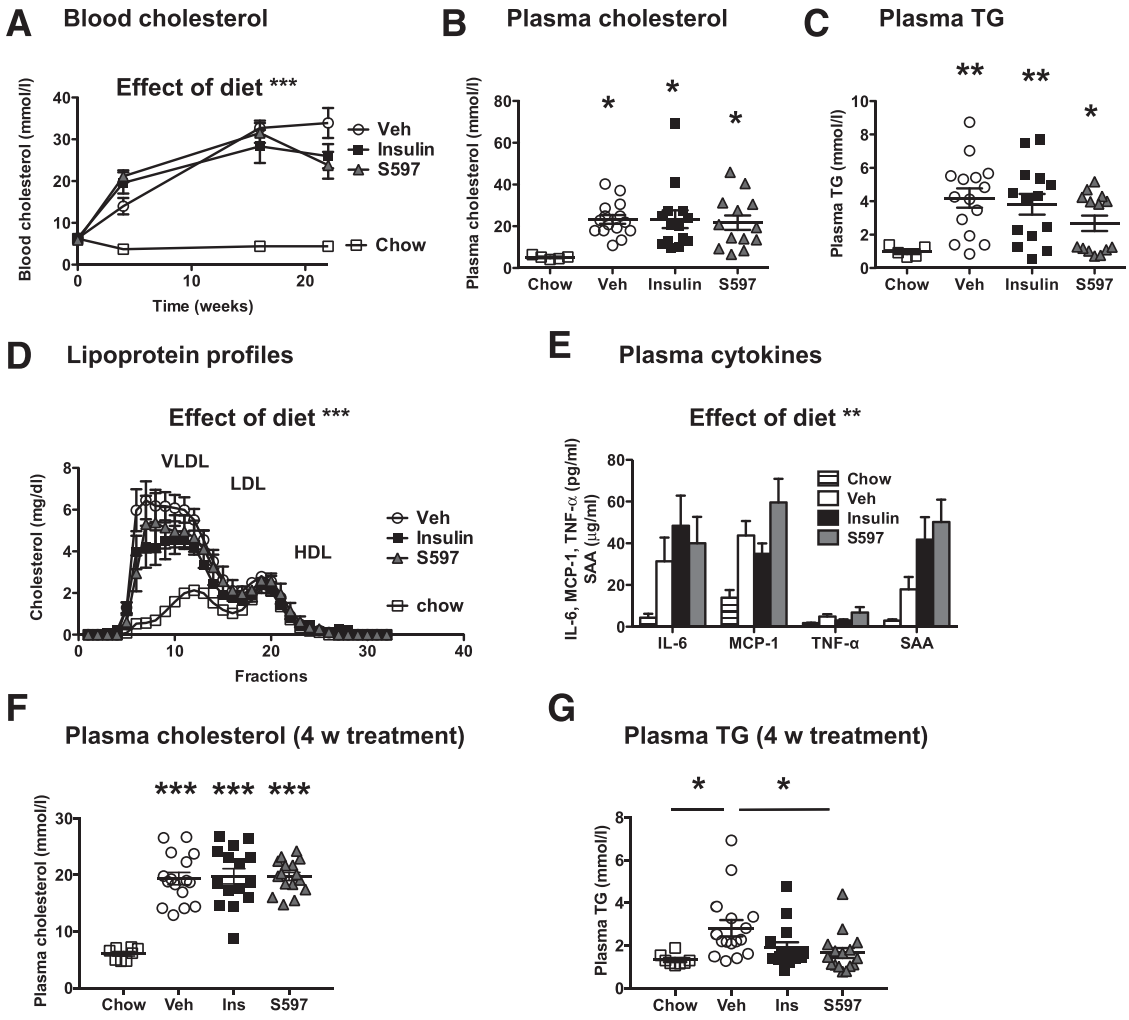

Figure 4—S597 does not reduce plasma cholesterol or systemic markers of inflammation. Blood cholesterol levels measured during the course of the study using a handheld cholesterol meter (*A*) or at the end of the 22-week study from plasma using a colorimetric assay (*B*). Veh, vehicle. *C*: Plasma triglycerides (TG) were measured using colorimetric assays from Wako at the end of the 22-week study. *D*: Lipoprotein profiles were assessed in three mice per group at the end of the 22-week study. *E*: Plasma IL-6, MCP-1 (CCL2), and TNF-α levels were measured using multiplex assays, and serum amyloid A (SAA) was measured by ELISA. Data are expressed as mean ± SEM (chow: $n = 5$; DDC groups: vehicle, $n = 14$; insulin, $n = 13$; S597, $n = 13$, unless otherwise specified). There were no significant differences between vehicle-treated mice, insulin-treated mice, and S597-treated mice. $^*P < 0.05$; $^{**}P < 0.01$; $^{***}P < 0.001$ vs. chow-fed mice by two-way ANOVA (*A*, *D*, and *E*) or one-way ANOVA (*B* and *C*). *F* and *G*: A cohort of mice were fed chow or DDC for 4 weeks and then injected twice daily with insulin or S597 for an additional 4 weeks while fed the DDC. Plasma cholesterol (*F*) and triglyceride (TG) (*G*) levels at the end of the study. Data are expressed as mean ± SEM (chow: $n = 8$; DDC groups: vehicle, $n = 16$; insulin, $n = 15$; S597, $n = 16$). w, weeks. $^*P < 0.05$; $^{***}P < 0.001$ vs. chow-fed mice or as indicated by one-way ANOVA.

bone marrow hematopoietic stem cells. S597 appears to interrupt leukocytosis at the earliest stages of hematopoiesis by inhibiting IR-Erk activation in bone marrow stem cells in this mouse model of metabolic syndrome (Fig. 6*K*). In addition to suppressing insulin-induced Erk activation, S597 could potentially suppress Erk activation through Akt (44), an effect that would be less pronounced for insulin, which activates both Akt and Erk. Although S597 inhibited the effect of insulin on Akt activation in the non-atherosclerotic aorta in vivo, that this action significantly contributed to the antiatherosclerotic effect of S597 is unlikely because vascular Akt1, the main Akt isoform expressed in endothelial cells and smooth muscle cells (45), prevents atherosclerosis (46). However, we cannot rule out that S597's action on other cell types or through other mechanisms could be involved in mediating its atheroprotective

euthanasia to assess insulin resistance by measuring hepatic p-Akt (*O*) and p-GSK3β (*P*). Data are expressed as mean ± SEM (chow: $n = 5$; DDC groups: vehicle, $n = 14$; insulin, $n = 13$; S597, $n = 13$, unless otherwise specified). $^{**}P < 0.01$, $^{***}P < 0.001$, two-way ANOVA, as indicated (*A–N*); $^*P < 0.05$, $^{**}P < 0.01$ vs. chow-fed mice by one-way ANOVA (*O*).

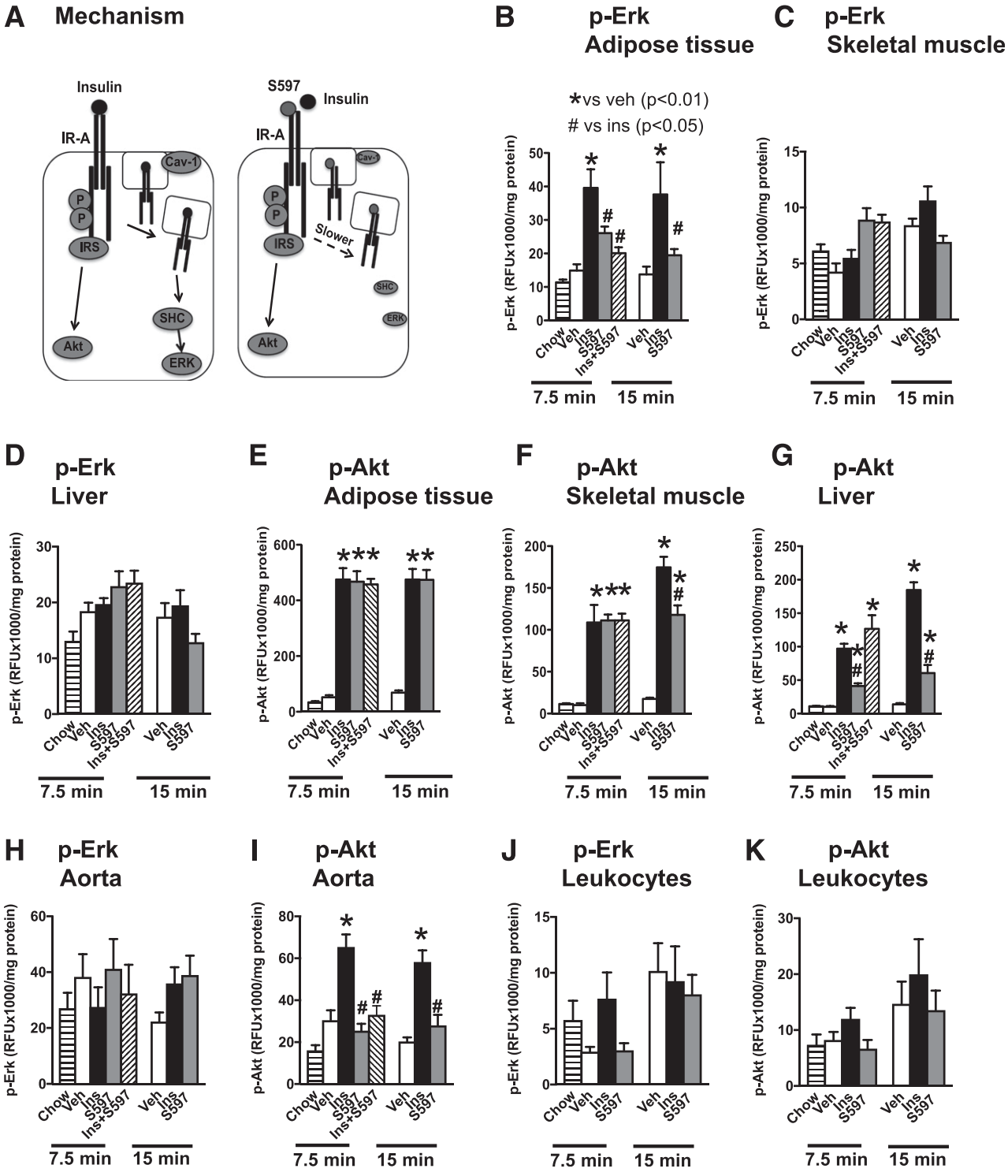

Figure 5—Differential signaling induced by S597 and insulin in vivo. *A*: Schematic representation of S597's action and induced downstream signaling based on previously published in vitro data. IRS, insulin receptor substrate; P, phosphate group. *B–K*: Male *Ldlr*$^{-/-}$ mice were fed chow or DDC for 4 weeks and then were treated with vehicle (Veh), insulin (Ins), or S597 twice daily for an additional 4 weeks. Mice were euthanized 7.5 or 15 min after the last injection. Adipose tissue p-Erk (*B*), skeletal muscle p-Erk (*C*), hepatic p-Erk (*D*), adipose tissue p-Akt (*E*), skeletal muscle p-Akt (*F*), hepatic p-Akt (*G*), aortic p-Erk (*H*), aortic p-Akt (*I*), blood leukocyte p-Erk (*J*), and blood leukocyte p-Akt (*K*) were determined using Alpha *Sure*Fire ELISAs. RFU, relative fluorescence units. Data are expressed as mean ± SEM (n = 8). *$P < 0.01$ vs. vehicle; #$P < 0.05$ vs. insulin, as indicated by one-way ANOVA.

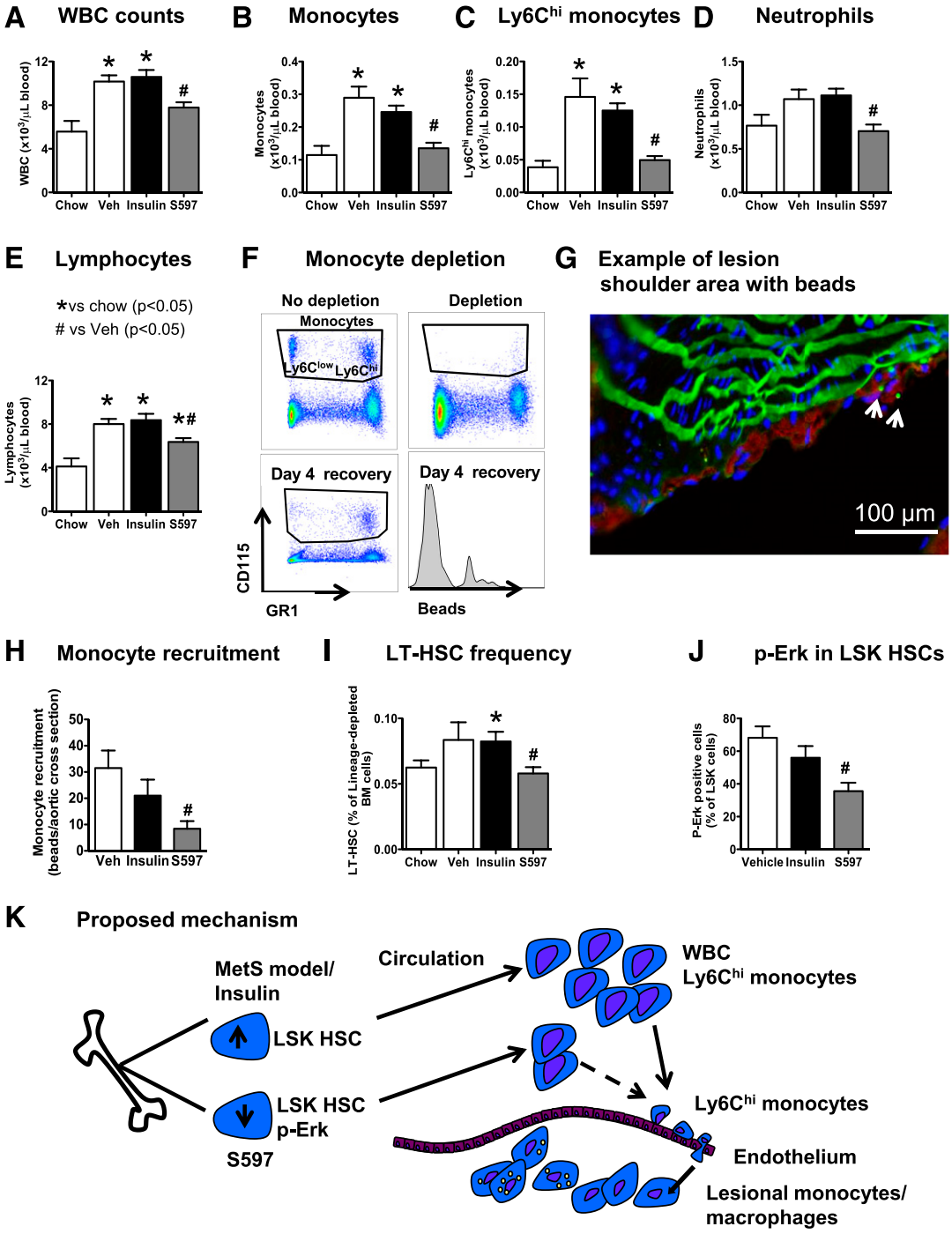

Figure 6—S597 prevents leukocytosis and Ly6C^{hi} monocyte accumulation in lesions and reduces numbers and p-Erk in bone marrow hematopoietic stem cells. *A–E*: Mice were injected for 4 weeks with vehicle (Veh), insulin, or S597. Blood was collected from the retro-orbital plexus under isoflurane sedation with EDTA as an anticoagulant. White blood cell (WBC) counts (*A*) were determined using a Hemavet automated counter. Total blood monocytes (*B*), Ly6C^{hi} (Gr1^{hi} CD115^{+}) monocytes (*C*), neutrophils (*D*), and lymphocytes (*E*) were determined by flow cytometry and normalized to total WBC count. Monocytes were depleted in mice with established atherosclerotic lesions after 10 days of treatment with vehicle, insulin, or S597. Deletion and frequency of labeling was similar between the treatment groups. *F*: Representative flow cytometric plots during monocyte depletion and recovery. Ly6C^{hi} monocytes appear in the upper right field and Ly6C^{lo} monocytes appear in the upper left field in each panel. *G*: Example of bead-positive CD68^{+} (red) macrophages in an atherosclerotic lesion. Beads are indicated by arrows. *H*: Quantification of bead-positive monocyte recruitment to lesions. *I*: Long-term hematopoietic stem cells (LT-HSC) frequency in bone marrow determined by flow cytometry. *J*: Lineage^{-} CD117^{+} Sca-1^{+} (LSK) hematopoietic stem cells (HSC) (the population that contains both LT-HSC and eGMP) were sorted and then stimulated with vehicle, insulin, or S597 for 7.5 min and stained for intracellular p-Erk (n = 13). Data were analyzed with repeated-measures ANOVA. *K*: Proposed mechanism for how S597 protects against advanced atherosclerosis in the model of metabolic syndrome (MetS). Data are expressed as mean ± SEM (*A–E*: chow, n = 8; all DDC groups, n = 16; *F–I*: n = 4–5). *$P < 0.05$ vs. chow; #$P < 0.05$ vs. vehicle, as indicated by one-way ANOVA.

effects. For example, it is possible that S597 might alter endothelial nitric oxide synthase activation, lower blood pressure, alter the innate immune reprogramming that contributes to myelopoiesis in fat-fed mice (47), or exert other systemic effects not investigated in this study. Future experiments in which different phosphorylation or docking sites in the IR (48) are mutated in cell-type specific manners might be informative in providing further mechanistic insight into the atheroprotective action of S597.

In summary, selective activation of the IR-Akt axis provides a novel conceptual framework for how differential signaling downstream of the IR could provide new treatment strategies for metabolic syndrome, T2DM, and associated CVD.

Acknowledgments. The authors thank Ricky Rualo and Shari Wang (University of Washington) and Marianne Schiødt (Novo Nordisk A/S) for analyses of experiments. They also thank Dr. Lauge Schäffer (Novo Nordisk A/S) for producing S597.

Funding. This study was partly supported by National Institutes of Health grants from the Division of Intramural Research, National Institute of Allergy and Infectious Diseases (T32-AI-106677 to J.M.D. and R01-AI-081948 to J.A.H.), National Heart, Lung, and Blood Institute (R01-HL-062887, P01-HL-092969, and R01-HL-126028 to K.E.B.), and National Institute of Diabetes and Digestive and Kidney Diseases (P30-DK-017047 and P30-DK-035816).

Duality of Interest. J.E.K. was supported by a Science Talent Attraction and Recruitment (STAR) Postdoc Fellowship from Novo Nordisk A/S. S.D.B., B.F.H., and G.S.O. are employed by Novo Nordisk A/S.

Author Contributions. J.E.K., F.K., S.B., J.M.D., M.S.-A., and V.K. performed experiments. J.E.K. and K.E.B. analyzed data and wrote the manuscript. A.C. provided assistance with lipid analyses and edited the manuscript. S.D.B., J.A.H., and B.F.H. contributed to the study design and the preparation of the manuscript. G.S.O. and K.E.B. designed and directed the study. All authors reviewed the manuscript and provided final approval for submission. K.E.B. is the guarantor of this work and, as such, had full access to all the data in the study and takes responsibility for the integrity of the data and the accuracy of the data analysis.

References

1. Lee CD, Folsom AR, Nieto FJ, Chambless LE, Shahar E, Wolfe DA. White blood cell count and incidence of coronary heart disease and ischemic stroke and mortality from cardiovascular disease in African-American and white men and women: atherosclerosis risk in communities study. Am J Epidemiol 2001;154:758–764

2. Nagareddy PR, Murphy AJ, Stirzaker RA, et al. Hyperglycemia promotes myelopoiesis and impairs the resolution of atherosclerosis. Cell Metab 2013;17:695–708

3. Nagareddy PR, Kraakman M, Masters SL, et al. Adipose tissue macrophages promote myelopoiesis and monocytosis in obesity. Cell Metab 2014;19:821–835

4. Kahn SE, Hull RL, Utzschneider KM. Mechanisms linking obesity to insulin resistance and type 2 diabetes. Nature 2006;444:840–846

5. Biddinger SB, Hernandez-Ono A, Rask-Madsen C, et al. Hepatic insulin resistance is sufficient to produce dyslipidemia and susceptibility to atherosclerosis. Cell Metab 2008;7:125–134

6. Han S, Liang CP, Westerterp M, et al. Hepatic insulin signaling regulates VLDL secretion and atherogenesis in mice. J Clin Invest 2009;119:1029–1041

7. Rask-Madsen C, Li Q, Freund B, et al. Loss of insulin signaling in vascular endothelial cells accelerates atherosclerosis in apolipoprotein E null mice. Cell Metab 2010;11:379–389

8. Han S, Liang CP, DeVries-Seimon T, et al. Macrophage insulin receptor deficiency increases ER stress-induced apoptosis and necrotic core formation in advanced atherosclerotic lesions. Cell Metab 2006;3:257–266

9. Baumgartl J, Baudler S, Scherner M, et al. Myeloid lineage cell-restricted insulin resistance protects apolipoproteinE-deficient mice against atherosclerosis [published correction appears in Cell Metab 2006;3:469]. Cell Metab 2006;3:247–256

10. Li S, Brown MS, Goldstein JL. Bifurcation of insulin signaling pathway in rat liver: mTORC1 required for stimulation of lipogenesis, but not inhibition of gluconeogenesis. Proc Natl Acad Sci U S A 2010;107:3441–3446

11. Kasuga M, Zick Y, Blithe DL, Crettaz M, Kahn CR. Insulin stimulates tyrosine phosphorylation of the insulin receptor in a cell-free system. Nature 1982;298:667–669

12. Schäffer L. A model for insulin binding to the insulin receptor. Eur J Biochem 1994;221:1127–1132

13. Schäffer L, Brissette RE, Spetzler JC, et al. Assembly of high-affinity insulin receptor agonists and antagonists from peptide building blocks. Proc Natl Acad Sci U S A 2003;100:4435–4439

14. Jensen M, Hansen B, De Meyts P, Schäffer L, Ursø B. Activation of the insulin receptor by insulin and a synthetic peptide leads to divergent metabolic and mitogenic signaling and responses. J Biol Chem 2007;282:35179–35186

15. Rajapaksha H, Forbes BE. Ligand-binding affinity at the insulin receptor isoform-A and subsequent IR-A tyrosine phosphorylation kinetics are important determinants of mitogenic biological outcomes. Front Endocrinol (Lausanne) 2015;6:107

16. Subramanian S, Han CY, Chiba T, et al. Dietary cholesterol worsens adipose tissue macrophage accumulation and atherosclerosis in obese LDL receptor-deficient mice. Arterioscler Thromb Vasc Biol 2008;28:685–691

17. Averill MM, Barnhart S, Becker L, et al. S100A9 differentially modifies phenotypic states of neutrophils, macrophages, and dendritic cells: implications for atherosclerosis and adipose tissue inflammation. Circulation 2011;123:1216–1226

18. Buechler MB, Teal TH, Elkon KB, Hamerman JA. Cutting edge: type I IFN drives emergency myelopoiesis and peripheral myeloid expansion during chronic TLR7 signaling. J Immunol 2013;190:886–891

19. Tacke F, Alvarez D, Kaplan TJ, et al. Monocyte subsets differentially employ CCR2, CCR5, and CX3CR1 to accumulate within atherosclerotic plaques. J Clin Invest 2007;117:185–194

20. Askari B, Carroll MA, Capparelli M, Kramer F, Gerrity RG, Bornfeldt KE. Oleate and linoleate enhance the growth-promoting effects of insulin-like growth factor-I through a phospholipase D-dependent pathway in arterial smooth muscle cells. J Biol Chem 2002;277:36338–36344

21. Lewis KE, Kirk EA, McDonald TO, et al. Increase in serum amyloid A evoked by dietary cholesterol is associated with increased atherosclerosis in mice. Circulation 2004;110:540–545

22. Hansen BF, Glendorf T, Hegelund AC, et al. Molecular characterisation of long-acting insulin analogues in comparison with human insulin, IGF-1 and insulin X10. PLoS One 2012;7:e34274

23. Akopian D, Medh JD. Simultaneous isolation of total cellular lipids and RNA from cultured cells. Biotechniques 2006;41:426, 428, 430

24. Renard CB, Kramer F, Johansson F, et al. Diabetes and diabetes-associated lipid abnormalities have distinct effects on initiation and progression of atherosclerotic lesions. J Clin Invest 2004;114:659–668

25. MacDougall ED, Kramer F, Polinsky P, et al. Aggressive very low-density lipoprotein (VLDL) and LDL lowering by gene transfer of the VLDL receptor combined with a low-fat diet regimen induces regression and reduces macrophage content in advanced atherosclerotic lesions in LDL receptor-deficient mice. Am J Pathol 2006;168:2064–2073

26. Kanter JE, Kramer F, Barnhart S, et al. Diabetes promotes an inflammatory macrophage phenotype and atherosclerosis through acyl-CoA synthetase 1. Proc Natl Acad Sci U S A 2012;109:E715–E724

27. Chang MY, Olin KL, Tsoi C, Wight TN, Chait A. Human monocyte-derived macrophages secrete two forms of proteoglycan-macrophage colony-stimulating factor that differ in their ability to bind low density lipoproteins. J Biol Chem 1998;273:15985–15992

28. Tsuchiya K, Tanaka J, Shuiqing Y, et al. FoxOs integrate pleiotropic actions of insulin in vascular endothelium to protect mice from atherosclerosis. Cell Metab 2012;15:372–381

29. Li X, Gonzalez O, Shen X, et al. Endothelial acyl-CoA synthetase 1 is not required for inflammatory and apoptotic effects of a saturated fatty acid-rich environment. Arterioscler Thromb Vasc Biol 2013;33:232–240
30. Han CY, Tang C, Guevara ME, et al. Serum amyloid A impairs the antiinflammatory properties of HDL. J Clin Invest 2016;126:266–281
31. Rosenfeld ME, Polinsky P, Virmani R, Kauser K, Rubanyi G, Schwartz SM. Advanced atherosclerotic lesions in the innominate artery of the ApoE knockout mouse. Arterioscler Thromb Vasc Biol 2000;20:2587–2592
32. Bailyes EM, Navé BT, Soos MA, Orr SR, Hayward AC, Siddle K. Insulin receptor/IGF-I receptor hybrids are widely distributed in mammalian tissues: quantification of individual receptor species by selective immunoprecipitation and immunoblotting. Biochem J 1997;327:209–215
33. Abbas A, Imrie H, Viswambharan H, et al. The insulin-like growth factor-1 receptor is a negative regulator of nitric oxide bioavailability and insulin sensitivity in the endothelium. Diabetes 2011;60:2169–2178
34. Frikke-Schmidt H, Pedersen TA, Fledelius C, et al. Treatment of diabetic rats with insulin or a synthetic insulin receptor agonist peptide leads to divergent metabolic responses. Diabetes 2015;64:1057–1066
35. Chait A, Goldberg I. Treatment of dyslipidemia in diabetes: recent advances and remaining questions. Curr Diab Rep 2017;17:112
36. Kocaman SA, Sahinarslan A, Kunak T, et al. The particular interactions of the traditional cardiovascular risk factors with different circulating specific leukocyte subtype counts in blood: an observational study. Anadolu Kardiyol Derg 2011;11:573–581
37. Tall AR, Yvan-Charvet L, Westerterp M, Murphy AJ. Cholesterol efflux: a novel regulator of myelopoiesis and atherogenesis. Arterioscler Thromb Vasc Biol 2012;32:2547–2552
38. Herishanu Y, Rogowski O, Polliack A, Marilus R. Leukocytosis in obese individuals: possible link in patients with unexplained persistent neutrophilia. Eur J Haematol 2006;76:516–520
39. Singer K, DelProposto J, Morris DL, et al. Diet-induced obesity promotes myelopoiesis in hematopoietic stem cells. Mol Metab 2014;3:664–675
40. Trottier MD, Naaz A, Li Y, Fraker PJ. Enhancement of hematopoiesis and lymphopoiesis in diet-induced obese mice. Proc Natl Acad Sci U S A 2012;109:7622–7629
41. Grimm RH Jr, Neaton JD, Ludwig W. Prognostic importance of the white blood cell count for coronary, cancer, and all-cause mortality. JAMA 1985;254:1932–1937
42. King GL, Park K, Li Q. Selective insulin resistance and the development of cardiovascular diseases in diabetes: the 2015 Edwin Bierman award lecture. Diabetes 2016;65:1462–1471
43. Thomas G, Tacke R, Hedrick CC, Hanna RN. Nonclassical patrolling monocyte function in the vasculature. Arterioscler Thromb Vasc Biol 2015;35:1306–1316
44. Rommel C, Clarke BA, Zimmermann S, et al. Differentiation stage-specific inhibition of the Raf-MEK-ERK pathway by Akt. Science 1999;286:1738–1741
45. Manning BD, Toker A. AKT/PKB signaling: navigating the network. Cell 2017;169:381–405
46. Fernández-Hernando C, Ackah E, Yu J, et al. Loss of Akt1 leads to severe atherosclerosis and occlusive coronary artery disease. Cell Metab 2007;6:446–457
47. Christ A, Günther P, Lauterbach MAR, et al. Western diet triggers NLRP3-dependent innate immune reprogramming. Cell 2018;172:162–175.e14
48. Myers MG Jr, White MF. Insulin signal transduction and the IRS proteins. Annu Rev Pharmacol Toxicol 1996;36:615–658